Original research

Biallelic mutations in the *TOGARAM1* gene cause a novel primary ciliopathy

Valeria Morbidoni,[1,2] Emanuele Agolini,[3] Kevin C Slep,[4] Luca Pannone,[5,6] Daniela Zuccarello,[1] Matteo Cassina,[1] Enrico Grosso,[7] Giorgia Gai,[7] Leonardo Salviati,[1,2] Bruno Dallapiccola,[8] Antonio Novelli,[3] Simone Martinelli,[5] Eva Trevisson [1,2]

► Additional material is published online only. To view please visit the journal online (http://dx.doi.org/10.1136/jmedgenet-2020-106833).

For numbered affiliations see end of article.

Correspondence to
Dr Eva Trevisson, Clinical Genetics Units, Women's and Children's Health, University of Padua, 35128 Padova, Veneto, Italy; eva.trevisson@unipd.it

Received 3 January 2020
Revised 23 June 2020
Accepted 26 June 2020
Published Online First 3 August 2020

ABSTRACT

Background Dysfunction in non-motile cilia is associated with a broad spectrum of developmental disorders characterised by clinical heterogeneity. While over 100 genes have been associated with primary ciliopathies, with wide phenotypic overlap, some patients still lack a molecular diagnosis.

Objective To investigate and functionally characterise the molecular cause of a malformation disorder observed in two sibling fetuses characterised by microphthalmia, cleft lip and palate, and brain anomalies.

Methods A trio-based whole exome sequencing (WES) strategy was used to identify candidate variants in the *TOGARAM1* gene. In silico, in vitro and in vivo (*Caenorhabditis elegans*) studies were carried out to explore the impact of mutations on protein structure and function, and relevant biological processes.

Results *TOGARAM1* encodes a member of the Crescerin1 family of proteins regulating microtubule dynamics. Its orthologue in *C. elegans*, *che-12*, is expressed in a subset of sensory neurons and localises in the dendritic cilium where it is required for chemosensation. Nematode lines harbouring the corresponding missense variant in *TOGARAM1* were generated by CRISPR/Cas9 technology. Although chemotaxis ability on a NaCl gradient was not affected, *che-12* point mutants displayed impaired lipophilic dye uptake, with shorter and altered cilia in sensory neurons. Finally, in vitro analysis of microtubule polymerisation in the presence of wild-type or mutant TOG2 domain revealed a faster polymerisation associated with the mutant protein, suggesting aberrant tubulin binding.

Conclusions Our data are in favour of a causative role of *TOGARAM1* variants in the pathogenesis of this novel disorder, connecting this gene with primary ciliopathy.

INTRODUCTION

Ciliopathies are a group of developmental and degenerative disorders characterised by cilia dysfunction.[1] Cilia can be distinguished into motile and primary types; both consist of a ciliary axoneme, which is composed by nine microtubule (MT) doublets and a basal body, a modified centriole that nucleates and anchors this structure to the cell. Motile cilia display an additional central pair of MTs.[2] Cilia structure and function require the orchestrated action of a number of proteins that are involved in several processes, including cilium assembly, regulation of protein entry into the cilium, protein transport, protein–protein interaction and cilia post-translational modifications (ie, polyglutamylation and acetylation of the axonemal MTs).[3]

Primary non-motile cilia are responsible for the transmission of multiple physical signals within cells, for cell-cycle control and modulation of signalling pathways, such as Hedgehog, Notch and Wnt signalling–planar cell polarity.[4] Since they are organelles present on most cell types, primary ciliary dysfunction tends to manifest with syndromic disorders displaying wide clinical heterogeneity, ranging from lethality to late-onset diseases. The clinical spectrum consists of primarily neurodevelopmental defects (with brain anomalies), retinal dystrophy and cystic renal disease. Additional symptoms include skeletal dysplasia, polydactyly, cleft lip/cleft palate and other craniofacial anomalies, sensorineural hearing loss and congenital fibrocystic disease of the liver and pancreas.[5]

This multisystemic involvement is paralleled by broad genetic heterogeneity, with over 100 genes associated with primary ciliopathies so far.[6] However, many patients still lack a molecular diagnosis[5 7] and, considering the growing number of ciliome components that currently consists of more than 420 proteins, it is anticipated that several other disorders with ciliopathic features will likely be ascribed to mutations in novel genes involved in ciliary structure and function.[1]

Phenotypic and genetic overlap between different ciliopathies is frequently observed, as in the case of Joubert (JBS, MIM #PS213300) and Meckel-Gruber (MKS, MIM #PS249000) syndromes, which represent the non-motile neurodevelopmental ciliopathies. Many causative genes are shared between these two disorders, suggesting that MKS may represent the extreme lethal phenotype of JBS.[8] Almost all these conditions are autosomal recessive traits, except for the X-linked *OFD1*-related disorders.

Here, we report biallelic mutations in the *TOGARAM1* gene in two fetuses displaying a phenotype consistent with a primary ciliopathy, overlapping in part Meckel-Gruber syndromes. This gene is highly conserved throughout evolution and its orthologue in nematodes (*che-12*) encodes a TOG domain–containing protein, belonging to the Crescerin family, whose members regulate MT

Check for updates

© Author(s) (or their employer(s)) 2021. No commercial re-use. See rights and permissions. Published by BMJ.

To cite: Morbidoni V, Agolini E, Slep KC, *et al*. *J Med Genet* 2021;**58**:526–533.

J Med Genet: first published as 10.1136/jmedgenet-2020-106833 on 3 August 2020. Downloaded from http://jmg.bmj.com/ on June 12, 2025 at Ist. Superiore Sanita Biblioteca. Protected by copyright, including for uses related to text and data mining, AI training, and similar technologies.

polymerisation through their TOG domain arrays. *che-12* localises in the dendritic cilium of a subset of sensory neurons that possess simple rod-like cilia.[9] Both TOGARAM1 and CHE-12 consist of four TOG domains. Since deletion mutants in *Caenorhabditis elegans* display a peculiar phenotype due to defects in functions mediated by sensory amphid and phasmid neurons,[9 10] and the novel missense substitution affects a highly conserved residue, we used *C. elegans* as an experimental model to investigate the impact of this variant on *che-12*/*TOGARAM1* function. In addition to in vivo data, in vitro MT polymerisation assays indicated an effect of the missense variant on TOG2–tubulin interaction.

PATIENTS AND METHODS

Genetic studies

All procedures were in accordance with the Declaration of Helsinki. Genetic studies were approved by the Bambino Gesù Children's Hospital ethics committees and written informed consents for molecular genetic analysis were obtained from parents.

Genomic DNA and RNA from the father's blood were extracted using standard methods. Library preparation and whole exome capture of DNA from fetal muscles and parents' blood were performed with the SeqCap EZ MedExome Kit (Roche) according to the manufacturer's protocol and sequenced on the NovaSeq550 platform (Illumina). The BaseSpace pipeline (Illumina) and the TGex software (LifeMap Sciences) were used for variants' calling and annotation. Sequencing data were aligned to the hg19 human reference genome. Functional impact of variants was analysed by Combined Annotation Dependent Depletion (CADD) V.1.4 and MutationTaster. Rare variants (minor allele frequency <0.1%) were filtered based on the gnomAD database. Based on the guidelines of the American College of Medical Genetics and Genomics (online supplementary table S1),[11] a minimum depth coverage of 30X was considered suitable for analysis. Variants were examined for coverage and Qscore (minimum threshold of 30) and visualised by the Integrative Genome Viewer. Mutations identified as pathogenic were confirmed by Sanger sequencing, following a standard protocol (BigDye Terminator V.3.1 Cycle Sequencing Kit; Applied Biosystems by Life Technologies).

One microgram of total RNA was retrotranscribed using the Superscript II (Thermo Fisher Scientific) and cDNA was amplified using appropriate primers including the fragment of *TOGARAM1* harbouring the c.3619C>T substitution (primers and PCR conditions are available on request). The PCR product was directly sequenced using Sanger method as described previously.

Structural modelling

Human Crescerin1 TOG2 residue Arg368 is equivalent to mouse Crescerin1 TOG2 residue Arg367. Mouse Crescerin1 TOG2 structure coordinates (Protein Data Bank code 5DN7 (10)) were used to visualise and render Arg367, which resides in the intra-HEAT repeat (HR) A loop (PyMOL (Schrodinger)). The mouse Crescerin1 residue Arg367 was mapped to the corresponding residue in *C. elegans* CHE-12 TOG2, Arg284.

Caenorhabditis elegans culture, genome editing and genetic crosses

Caenorhabditis elegans strains were grown monoxenically on Nematode Growth Medium (NGM) agar plates at 20°C, feeding *E. coli* OP50 bacteria.[12] Worm synchronisation was carried out with standard methods.[13] Wild-type N2 and SP1620 (*che-12 (mn389) V*) strains as well as OP50 bacteria were purchased from CGC (*Caenorhabditis* Genetics Center, University of Minnesota). The SP1620 strain carries a partial C-terminal deletion of *che-12*.[9] The LP177 strain (*unc-119(ed3) III; che-12(cp26[Δ1–1282+GFP+LoxP unc-119(+) LoxP]) V*), which harbours a whole deletion of *che-12*, was previously reported.[10]

The Alt-R CRISPR/Cas9 System (Integrated DNA Technologies) was used to perform genome editing in *C. elegans* in order to obtain *che-12* point mutant nematodes harbouring the missense variant p.Arg284Trp corresponding to the human substitution. Following published guidelines,[14] CRISPR RNAs (crRNAs) and DNA repair templates specific for *che-12* and *dpy-10 loci* were designed (sequences are listed in online supplementary table S2). Worm injections were carried out following a protocol modified from Paix *et al*.[15] Briefly, the distal gonad syncytium of young adult wild-type hermaphrodite animals was injected with a mix containing 115 ng/µL of crRNA and 37.5 ng/µL of ssODN (*dpy-10*) or 400 ng/µL of crRNA and 175 ng/µL of ssODN (*che-12*); for both *loci*, 750 ng/µL of Cas9 protein and 700 ng/µL of tracrRNA were added. The genome-edited lines were backcrossed twice with the wild-type strain to remove possible off-target effects introduced by the CRISPR/Cas9 editing. Worms were genotyped by EcoRV digestion of the PCR fragments spanning from exon 5 to exon 7, including the variant of interest (primers and PCR conditions are available on request). The missense substitution was confirmed by Sanger sequencing.

Two independent lines were used for each experiment. Males from the OH1392 strain, which carries the *gcy-5p::GFP* marker to specifically express GFP in the ASER neuron,[16] were crossed with hermaphrodites from *che-12*(*pan11*[Arg284Trp (AGA>TGG)]) *V*, *che-12*(*pan12*[Arg284Trp (AGA>TGG)]) *V* or *che-12 (mn389) V*. The genetic screening was performed among GFP-positive worms of the F2 generation, and worms carrying the p.Arg284Trp missense variant or the *che-12*(*mn389*) allele were screened.

Worm phenotypic characterisation

Chemotaxis and dye-uptake assays

Wild-type worms, *che-12*(*pan11*[Arg284Trp (AGA >TGG)]) *V* and *che-12*(*pan12*[Arg284Trp (AGA >TGG)] *V* point mutant nematodes, a strain carrying a truncated CHE-12 protein (SP1620) and one where *che-12* was totally ablated by CRISPR/Cas9 (LP177) were synchronised, grown on NGM plates until adulthood was reached and their capability to chemotax on a linear NaCl gradient was assayed as previously published.[10] Control isocratic plates were used to ensure that worm movements were totally random in the absence of a salt gradient.

The same strains were assayed for dye uptake with Vybrant CM-DiI (3H-Indolium, 5-[[[4-(chloromethyl)benzoyl]amino] methyl]-2-[3-(1,3-dihydro-3,3-dimethyl-1-octadecyl-2H-indol-2-ylidene)-1-propenyl]-3,3-dimethyl-1-octadecyl-, chloride; Thermo Fisher Scientific) or fluorescein-5-isothiocyanate (FITC) isomer I (Sigma-Aldrich). After synchronisation, worms were cultivated on NGM plates until adulthood and then incubated in M9 buffer containing a 1:1000 dilution of CM-DiI, while for FITC a final concentration of 0.4 mg/mL was tested, as previously described.[9] Nematodes were stained as reported.[10] Worms were then anaesthetised in M9 supplemented with 25 mM sodium azide and mounted live on 2% agarose pads on glass slides. FITC and Vybrant CM-DiI staining signals were acquired using FITC-specific and rhodamine-specific filters, respectively, focusing on the worm head region where amphid neurons lie,

J Med Genet: first published as 10.1136/jmedgenet-2020-106833 on 3 August 2020. Downloaded from http://jmg.bmj.com/ on June 12, 2025 at Ist. Superiore Sanita Biblioteca. Protected by copyright, including for uses related to text and data mining, AI training, and similar technologies.

using a Zeiss Axio Imager M1 fluorescence microscope with ×20 and ×40 magnification. For each genotype, the percentage of worms harbouring between one and four, between five and seven, and eight or more positive amphid neurons was calculated, and the results of different strains were compared using the χ^2 method.

Cilium length measurement

After being anaesthetised and mounted on glass slides as indicated previously, GFP-positive adult worms were imaged using a Zeiss LSM 800 confocal microscope in order to measure the length of ASER dendritic cilium. Images were acquired using a ×63 objective, zooming on the ASER cilium within the head's amphid bundle. Images were then analysed using the ImageJ software package. Cilium length values for each genotype were mediated, worms carrying the wild-type version of *che-12* were considered as one and other strains were expressed as fractions compared with it. Results of different strains were compared using the unequal variance t-test.

Transmission electron microscopy

Adult *C. elegans* hermaphrodites were prepared for the amphid dendritic cilia analysis at the transmission electron microscope using an optimised protocol based on what was previously reported.[10] First, worms were collected from agar plates with M9 buffer into 1.5 mL microcentrifuge tubes and then washed twice in M9 buffer in order to remove bacteria.

Samples were fixed in glutaraldehyde 2.5% in 0.1M sodium cacodylate buffer overnight at 4°C, postfixed in osmium tetroxide 1% for 1 hour at 4°C, and rinsed twice in 0.1M sodium cacodylate and once in deionised water. Samples were dehydrated in a graded series of ethanol solutions (25%, 50%, 75%, 100%), followed by three changes in propylene oxide, resin infiltrated gradually (3:1, 1:1, 1:3) and finally embedded in EMbed 812 (Electron Microscopy Sciences) epoxy resin. Ultrathin sections (70–80 nm) were cut with a Reichert-Yung Ultracut ultramicrotome, using a diamond knife (Diatome), collected on Formvar-coated slot grids and then stained with a saturated solution of uranyl acetate in 50% ethanol and Reynold's lead citrate. Samples were examined with a Tecnai G^2 (Fei-Thermo Fisher) transmission electron microscope operating at 100 kV and digital images were acquired using a Veleta (Olympus Soft Imaging Solutions) digital camera.

In vitro studies

TOG2 cloning, expression and purification

Mouse Crescerin1 TOG2 (residues 332–620) in pET28b[10] was used as a template for PCR sewing mutagenesis, yielding TOG2 (residues 332–620) Arg367Trp in pET28 (Millipore Sigma). The Arg367Trp mutation was verified by Sanger sequencing. Bacterial protein expression growths were performed in 3 L of LB media as described.[10] Wild-type and Arg367Trp TOG2-expressing cells were harvested (2100×*g* for 10 min), resuspended in 250 mL of buffer A (25 mM Tris pH 8.5, 300 mM NaCl, 15 mM imidazole, 0.1% (v/v) beta-mercaptoethanol), sonicated to lyse and 1 mM (final concentration) phenylmethylsulfonyl fluoride added. Lysate was centrifuged at 23 000×*g* for 45 min. Supernatant was loaded onto a 5 mL Ni^{2+}-nitriloacetic acid column (Qiagen) and washed with 300 mL of buffer A. Protein was then eluted using 50 mL of buffer B (buffer B=buffer A supplemented with 290 mM imidazole). Protein was concentrated and exchanged into 25 mM Tris pH 8.0, 250 mM KCl and 0.1% (v/v) beta-mercaptoethanol using a Millipore Ultrafree 10 000 MWCO concentrator. Protein was aliquoted, frozen and maintained at −80°C.

Table 1 Clinical features of the two fetuses

	Fetus 1	Fetus 2
General data		
Sex	Male	Male
TOP age	21	17
Weight	490 g	210 g
Length	28 cm	20 cm
Phenotype		
Severe cleft lip and palate	+	+
Microphthalmia (bilateral)	+	+
Hydrocephalus	Severe	Moderate
Lissencephaly	+	–
Cerebellar hypoplasia	–	+
Abdominal testes	+	–
Heart	Normal	Normal
Skeletal system	Normal	Normal
Prenatal genetic testing		
QF-PCR	Normal male	Normal male
Karyotype	n.p.	46,XY
CGH array	No result*	Normal male

*CGH-array analysis failed due to the poor DNA quality extracted from fetus 1 autoptic material.
–, absent; +, present; n.p., not performed; TOP, termination of pregnancy (gestational age expressed in weeks).

In vitro MT polymerisation assay

Tubulin polymerisation was monitored over time using a SPEX Fluorolog-3 spectrophotometer (Horiba Jobin Yvon) in T-format, high-voltage mode. The excitation and detection wavelengths were set at 350 nm, the excitation slit at 0.5 nm and the emission slit at 0.75 nm. The cuvette holder was maintained at 37°C. Lyophilised tubulin was solubilised according to the vendor's protocol (PurSolutions) and clarified at 4°C. Tubulin samples (18 µM final concentration (PurSolutions)) were prepared in the presence or absence of Crescerin1 TOG2 constructs, each at 3 µM final concentration, in polymerisation buffer (50 mM 2-(N-morpholine)ethanesulfonic acid (MES), pH 6.6, 3.4 M glycerol, 5 mM dithiothreitol, 1 mM ethylene glycol tetraacetic acid, 5 mM $MgSO_4$, 1 mM GTP) and incubated on ice for 8 min. The 270 µL samples were injected into a 4 mm path length quartz cuvette at room temperature and then immediately placed into the 37°C cuvette holder. Scattering was recorded at 350 nm in 1 s intervals over 1500 s. Experiments were performed in duplicate, yielding reproducible effects.

RESULTS

Clinical description and molecular analysis

Unrelated young parents (<35 years) with negative personal and family histories were referred to our Hospital following two second-trimester pregnancy terminations due to multiple fetal malformations, including microcephaly, severe cleft lip and palate, microphthalmia and brain malformations (table 1).

QF-PCR analysis on DNA from amniocytes excluded common aneuploidies on both fetuses. Chromosomal analysis and array-CGH in fetus 2 did not detect any anomaly. In order to identify the molecular defect underlying the condition in the two fetuses, whole exome sequencing (WES) analysis was carried out on DNA from fetus 2 and its parents. WES data

J Med Genet: first published as 10.1136/jmedgenet-2020-106833 on 3 August 2020. Downloaded from http://jmg.bmj.com/ on June 12, 2025 at Ist. Superiore Sanita Biblioteca. Protected by copyright, including for uses related to text and data mining, AI training, and similar technologies.

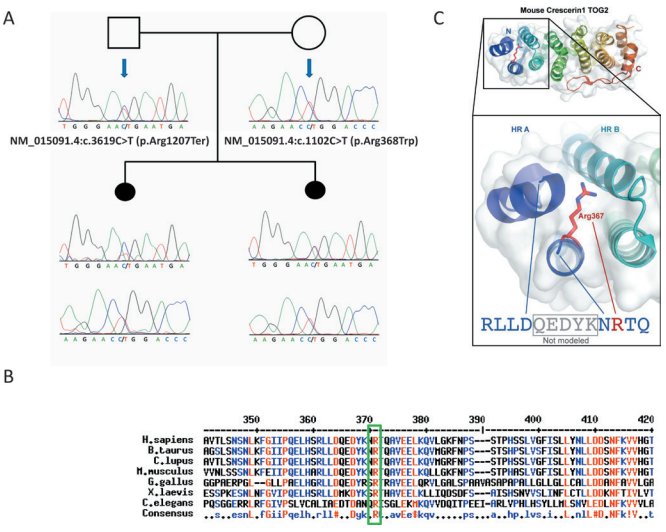

Figure 1 (A) Family pedigree showing the compound heterozygous genotype identified in the *TOGARAM1* (*FAM179B*) gene in two fetuses, NM_015091.4:c.1102C>T [p.(Arg368Trp)] and c.3619C>T [p.(Arg1207*)], inherited from the mother and father, respectively. (B) Alignments of human (NP_001295049.1), cattle (XP_024837862.1), dog (XP_013971352.1), African clawed frog (XP_018085990.1), mouse (NP_808473.2), chicken (XP_025006655.1) and *C. elegans* (NP_001256204.1) TOGARAM1 protein sequences highlighting that the arginine residue of interest is conserved among species (green box). (C) The crystal structure of mouse TOG2 domain (PDB database, http://www.rcsb.org/, accession number 5DN7) with 12 helices that pair into six tandem HRs (represented in different colours) and a final *C*-terminal β-hairpin depicted in red. In the zoomed region, the Arg367 residue of interest (intra-HR A loop), positioned at the start of HR A's second alpha-helix with its side chain engaging determinants in HR B. Intra-HR A loop residues 361–365 are disordered and were not modelled.

analysis (online supplementary table S1) identified a compound heterozygous genotype in the *TOGARAM1* (*FAM179B*) gene: NM_015091.4:c.1102C>T [p.(Arg368Trp)], and c.3619C>T [p.(Arg1207*)], which was confirmed also in fetus 1, with each variant being inherited from the mother and father, respectively (figure 1A).

The missense change p.(Arg368Trp) is not reported in the GnomAD database, it involves a highly conserved residue across species (figure 1B) and is predicted to be deleterious (scaled CADD score 26; MutationTaster score 0.996). This substitution can be classified as a variant of uncertain significance (variant of class 3 according to the ACMG criteria PM2 and PP3).[17] The nonsense variant p.(Arg1207*) is absent in GnomAD but is reported in the Exome Sequencing Project database with an allele frequency of 0.0001 in the European/American population. This variant introduces a premature stop at codon 1207 resulting in the production of a predicted truncated protein lacking 30% of the amino acid sequence. To evaluate the presence of nonsense-mediated mRNA decay (NMRD), we analysed RNA extracted from father's blood, who harbours the heterozygous nonsense variant: RT-PCR followed by Sanger sequencing of the fragment of *TOGARAM1* including the c.3619C>T substitution showed a biallelic expression, indicating that the mutant transcript is not significantly degraded (online supplementary figure S1).

Other variants identified by WES were not consistent with the clinical phenotype and were not considered further.

Structural modelling

To gain insight into the human Crescerin1 p.Arg368Trp substitution, we examined the equivalent residue in the structure of the mouse Crescerin1 TOG2 domain, which is residue Arg367 (Protein Data Bank code 5DN7[10]). This amino acid lies within the TOG2 domain (online supplementary figure S2) and resides in the intra-HEAT repeat (HR) A loop, positioned at the start of HR A's second alpha-helix with its side chain engaging determinants in HR B (figure 1C). In TOG domains of the XMAP215 family of MT polymerases, the intra-HR A loop contains key residues, including a conserved tryptophan, which are involved in tubulin binding.[18 19] In the mouse Crescerin1 TOG2 structure, the intra-HR A loop residues 361–365 are disordered and were not modelled. Within this set, Tyr364 is predicted to be the functional equivalent of the tryptophan found in XMAP215 TOG domains. On binding tubulin, we predict the disordered intra-HEAT A loop would become ordered and pack against Arg367. The Arg367Trp change is predicted to alter tubulin binding by either disrupting the conformation or dynamics of the 361–365 loop region, or modulating any direct interaction residue 367 may have with tubulin. Across the Crescerin family, the arginine residue is well conserved, extending to the nematode where it maps to *C. elegans* CHE-12 residue Arg284 (figure 1B).

Generation of a *C. elegans* model

TOGARAM1 is a member of a protein family conserved in ciliated/flagellated eukaryotes ranging from mammals to unicellular eukaryotes, but is absent in non-ciliated ones, like yeast.[10] In *C. elegans*, the role of the orthologue gene *che-12* has been deeply characterised, and both hypomorphic and knock-out mutants showing discernible phenotypes (including short amphid cilia, aberrant ultrastructure of the axoneme, defective chemotaxis and dye uptake) have been generated. Particularly, the following three partial C-end deletion mutants (*che-12(e1812)*, *che-12(mn389)*, *che-12(mn399)*) harbour distinct mutations affecting the region downstream of the TOG2 domain, similar to the Arg1207* variant found in our family (online supplementary figure S2): they display an analogous phenotype that resembles what was observed in the full-deletion mutant, although to a lesser extent.[9 10]

Thus, we employed *C. elegans* as a model to investigate the effects of the missense variant on TOGARAM1 function. CRISPR/Cas9 technology was used to generate point mutant nematodes harbouring the CHE-12 p.Arg284Trp substitution. Three independent lines were obtained, *che-12*(*pan11*[Arg284Trp (AGA >TGG)]) *V*, *che-12*(*pan12*[Arg284Trp (AGA >TGG)]) *V* and *che-12*(*pan13*[Arg284Trp (AGA >TGG)]) *V*.

Chemotaxis and dye-uptake assay

Partial and total deletions of *che-12* in *C. elegans* cause the impairment of specific functions mediated by amphid and phasmid sensory cilia where *che-12* is expressed, including chemotaxis towards soluble attractants and lipophilic dye uptake.[9 10] Therefore, we assessed these behavioural phenotypes in worms harbouring the p.Arg284Trp variant.

First, we measured the ability of mutant animals to chemotax along a linear NaCl gradient. Hypomorphic and null mutants, which display an impaired ability to sense the NaCl gradient with a similar pattern of migration in gradient and control plates, were used as controls. *che-12*(*pan11*[Arg284Trp (AGA >TGG)]) *V* and *che-12*(*pan12*[Arg284Trp (AGA >TGG)]) *V* lines behaved similar to wild-type worms, being strongly attracted to the high-salt end (sector 1) in gradient plates (figure 2A).

J Med Genet: first published as 10.1136/jmedgenet-2020-106833 on 3 August 2020. Downloaded from http://jmg.bmj.com/ on June 12, 2025 at Ist. Superiore Sanita Biblioteca. Protected by copyright, including for uses related to text and data mining, AI training, and similar technologies.

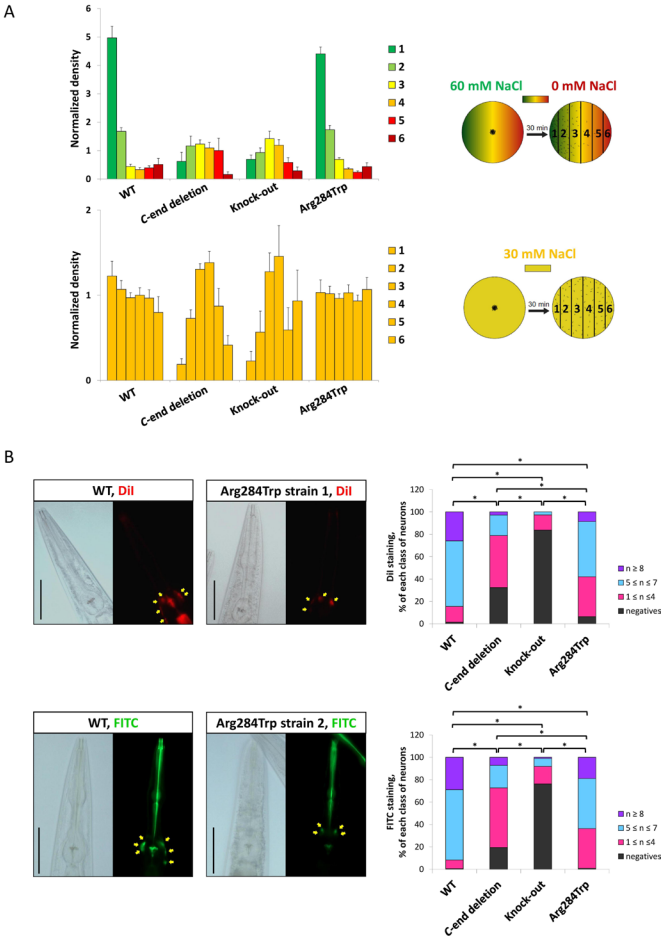

Figure 2 (A) Chemotaxis assay performed on wild-type worms (N2), *C*-end deletion mutant (SP1620), knock-out mutant (LP177), Arg284Trp point mutants (strain 1: *che-12*(*pan11*[Arg284Trp (AGA >TGG)]) *V* and strain 2: *che-12*(*pan12*[Arg284Trp (AGA >TGG)]) *V*, whose results were mediated). Animals were synchronised and once adults they were seeded in the centre of control isocratic plates prepared with 30 mM NaCl (below), or with a linear 0–60 mM NaCl gradient (above). In both cases, after 30 min of free run, plates were cooled down and the normalised density for each of the six parallel sectors of the plate (depicted in distinct colours nearby each histogram) was counted. The graphs represent the mean of at least three experiments and the error bars show the SE of the mean. (B) Lipophilic dye staining. Above the results of Vybrant CM-DiI staining and below those of FITC staining. For each dye, representative images of wild-type (WT) (N2) and Arg284Trp point mutant strains 1 and 2 (genotypes are the same as above) are shown on the left with yellow arrows indicating stained amphid neurons (scale bar, 50 µm), while on the right the quantification of stained worms in each strain is reported as the mean of two independent experiments (Arg284Trp strains 1 and 2 were mediated as above). Worms were divided into four categories (each shown as a percentage on the total): negative, those harbouring between 1 and 4 ($1 \leq n \leq 4$), 5 and 7 ($5 \leq n \leq 7$) and 8 or more ($n \geq 8$) positive amphid neurons. A minimum of 71 and 139 animals were imaged after DiI and FITC assay, respectively. The χ^2 test was used to compare the distribution of positive worms in different strains; *$p<10^{-7}$.

Second, worms' uptake of lipophilic dye was investigated by incubating nematodes with Vybrant CM-DiI and FITC, similarly to what was previously performed[9 10]: counting the number of positive amphid neurons within each animal revealed that point mutant strains display an altered distribution of worms that took up the dye, with a significant increase of animals with few stained neurons, which was less penetrant compared with *C*-end deletion and knock-out nematodes (figure 2B).

Cilium length measurement and ultrastructural analysis

The ASER neuron is an amphid sensory cell that possesses a simple finger-like cilium.[20] Worms harbouring partial or total *che-12* deletions were found to have a shorter ASER cilium with poorly defined MT architecture at proximal ends and no apparent distal MT structures, thus highlighting the relevance of this protein for sensory cilia length and ultrastructure.[9 10]

To determine whether the novel human missense variant modelled on *che-12* could affect cilium length and ultrastructure, we analysed point mutant animals by confocal fluorescence and electron microscopy (EM).

First, we measured the length of the ASER dendritic cilium in worms harbouring the *che-12* p.Arg284Trp missense variant or the *che-12*(*mn389*) allele (strain SP1620) and in wild-type animals by confocal microscopy, after crossing them with a line expressing GFP in the ASER neuron (under the control of the *gcy-5* promoter).

Of note, point mutant nematodes display a significantly shorter cilium (0.88 ± 0.02 vs 1 ± 0.03 of normalised ASER cilium length of wild-type worms) that was however longer compared with *che-12* hypomorphic mutants (0.74 ± 0.02) (figure 3A).

We also crossed the *che-12* knock-out animals with the mutant worms carrying the Arg284Trp missense variant and expressing the GFP in the ASER neuron as shown previously: we obtained the hemizygous *ntIs1 [gcy-5p::GFP+lin-15(+)] che-12 pan12/cp26[Δ1–1282+GFP+LoxP unc-119(+) LoxP] V* strain, which showed a further shortening of the ASER dendritic cilium (0.82 ± 0.01) (figure 3A).

We then performed ultrastructural analysis by EM, examining the amphid channel cilia: again, we compared cilium structure of *che-12* point mutant worms with that of wild-type and knock-out animals. EM data revealed the presence of disorganised cilium architecture, which was more evident in its distal part, as previously reported for the knock-out strain.[10] In agreement with results from fluorescence microscopy findings, alterations observed in the point mutant were less pronounced compared with those found in the null mutant (figure 3B).

In vitro polymerisation assay

We next used a tubulin polymerisation light scattering assay to determine if the human Crescerin1 TOG2 Arg368Trp variant had an effect on TOG2–tubulin interactions. Prior work demonstrated that mouse Crescerin1 TOG2 could potentiate MT polymerisation in an in vitro light scattering assay.[10] We generated a mouse TOG2 construct containing the corresponding Arg367Trp mutation, expressing the recombinant protein *in E. coli*, and purified the domain to homogeneity. The mutant TOG2 construct behaved similar to the wild-type TOG2 construct and its solubility indicated that the mutation did not compromise the domain's integrity (figure 3C).

In the light scattering assay, tubulin polymerisation activity was monitored over time (25 min) using its ability to scatter light at 350 nm as a readout. Lyophilised tubulin was solubilised and used in the experiments, which yielded immediate polymerisation kinetics once placed at 37°C, likely due to small tubulin aggregates in the sample that served as nucleation seeds. Relative to this tubulin-alone baseline control, the addition of wild-type mouse Crescerin1 TOG2 to the solution increased the rate of tubulin polymerisation as previously observed.[10] The addition of the mouse Crescerin1 TOG2 Arg367Trp mutant

J Med Genet: first published as 10.1136/jmedgenet-2020-106833 on 3 August 2020. Downloaded from http://jmg.bmj.com/ on June 12, 2025 at Ist. Superiore Sanita Biblioteca. Protected by copyright, including for uses related to text and data mining, AI training, and similar technologies.

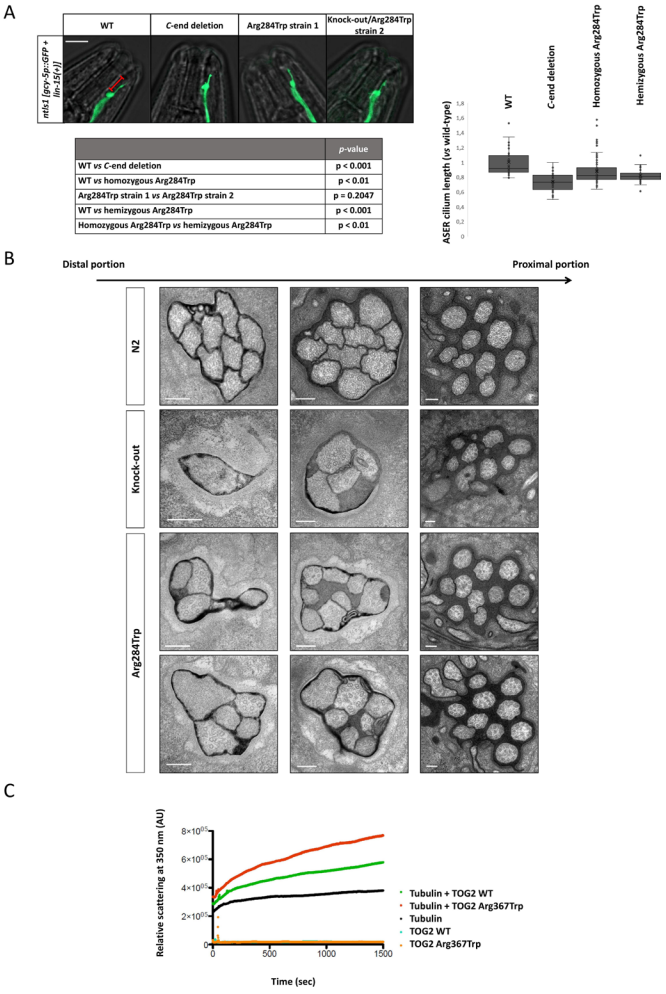

Figure 3 (A) On the left, exemplifying images of ASER GFP reporter worms carrying the homozygous wild-type *che-12* allele (WT), the homozygous *C*-end deletion mutant (SP1620), or the homozygous Arg284Trp point mutants strain 1, and the hemizygous Arg284Trp point mutant. A red brace specifies the cilium portion considered for quantification (Arg284Trp strains 1 and 2 were mediated as above, scale bar, 5 µm). On the right, cilium length measurements, normalised for each strain to the wild-type *che-12*, were represented in a box-and-whisker plot. At least 37 animals were imaged in all groups and error bars indicate variability outside the upper and lower quartiles. Values were compared using the unequal variance t-test and the results of the statistical analysis are reported in the table. (B) Cross-sectional transmission electron micrographs of amphid dendritic cilia in wild-type, *che-12* knock-out and Arg284Trp point mutant nematodes. Three portions of cilia are shown, ranging from a distal section (left), to a proximal one (right); two Arg284Trp point mutants are represented in the images (scale bar, 200 nm). A schematic indicating the position of cross-sections are shown in online figure supplementary S3. (C) Light scattering assay. Tubulin polymerisation activity was monitored over time (25 min) using its ability to scatter light at 350 nm as a readout. Lyophilised tubulin was solubilised and used in the experiments, with or without the mouse Crescerin1 wild-type or Arg367Trp mutant TOG2. Wild-type TOG2 and the Arg367Trp mutant construct were also run alone, without tubulin, as controls of the experiment.

construct increased the rate of tubulin polymerisation even further (figure 3C). Neither wild-type TOG2 nor the Arg367Trp mutant construct scattered light when run alone, indicating that the scattering is due to tubulin polymerisation, and potentially MT–TOG interactions. Collectively, these data suggest that the Arg367Trp mutation alters TOG2–tubulin interactions.

DISCUSSION

In this study, we report biallelic mutations in the *TOGARAM1* gene, which encodes a protein required for cilia function, as a novel cause of primary ciliopathy in humans, and performed the functional characterisation of these variants in a multicellular organism.

TOGARAM1 (TOG array regulator of axonemal microtubules 1) was initially identified as a protein able to bind tubulin and regulate MT dynamics (formerly named FAM179B, KIAA0423). In fact, it shows discontinuous sequence similarity to the TOG1 domain of the cytoskeletal linker protein 170–associated protein (CLASP) MT-associated proteins and belongs to the Crescerin family, which is conserved in ciliated/flagellated eukaryotes ranging from mammals to unicellular organisms. The murine orthologue, Crescerin1, harbours four domains, and the crystal structure of the second domain was determined, revealing 12 helices that pair into six tandem HRs and stack, forming a solenoid that conforms to a canonical TOG architecture with conserved intra-HEAT loops. Consequently, it was designated as a TOG domain, in particular TOG2, proving that Crescerin represents a third, unique TOG domain–containing protein family.[10]

WES analysis identified biallelic variants in *TOGARAM1* in two sibling fetuses affected by a severe malformation disorder overlapping in part the Meckel-Gruber syndrome's phenotype: a missense variant, [p.(Arg368Trp], and a truncating allele. Segregation analysis confirmed that each variant was inherited from an unaffected parent. The missense substitution is classified as a variant of unknown significance (class 3 according to ACMG criteria[17]) since it is extremely rare (not reported in the gnomAD and dbSNP databases). Nevertheless, this residue is highly conserved throughout evolution and both predictive software and modelling analyses support its pathogenicity due to the possible perturbation of HRs in the TOG2 domain. In fact, the arginine residue lies just under the first tubulin-binding loop of the domain and the substitution with a tryptophan could alter its orientation, thus affecting tubulin binding activity, or at least the ability of the first and second HRs to correctly pack together.

In order to validate the pathogenicity of the missense variant, we took advantage of the nematode *C. elegans*, which, unlike non-ciliated organisms like yeast, possesses CHE-12, a characterised member of the Crescerin family that represents the orthologue of human TOGARAM1. *che-12* is expressed in some amphid and phasmid neurons, a subset of sensory cells located in the worm's head and tail, respectively, and localises in the dendritic cilium where it is required for proper chemosensation. Previous studies on null and hypomorphic worm mutants found that the absence of CHE-12 causes a severe phenotype, with shorter and disorganised dendritic cilia. In addition, different *C*-terminal end mutants (alleles *e1812*, *mn389* and *mn399*) show cilia structural alterations and defects in behaviours normally controlled by amphid neurons (eg, chemotaxis ability, amphid neuron staining), but to a lesser extent compared with the null mutants, indicating that they retain partial CHE-12 function and thus are hypomorphic.[9 10]

Point mutant *C. elegans* strains were generated using the CRISPR/Cas9 technology in order to model the novel missense variant in the corresponding CHE-12 residue. We performed a phenotypic characterisation of behaviours controlled by amphid neurons. Although the ASER-mediated capability

J Med Genet: first published as 10.1136/jmedgenet-2020-106833 on 3 August 2020. Downloaded from http://jmg.bmj.com/ on June 12, 2025 at Ist. Superiore Sanita Biblioteca. Protected by copyright, including for uses related to text and data mining, AI training, and similar technologies.

of point mutants to chemotax on a linear NaCl gradient was preserved, point mutant strains show a defective lipophilic dye filling phenotype, with a significant increase of animals with few stained neurons compared with WT animals, although not as striking as in C-end deletion and knock-out nematodes.

In particular, while they still properly chemotax along a NaCl gradient, their ability to take up and concentrate lipophilic dyes is reduced, suggesting a hypomorphic effect of the missense variant.

To get further insight into the worm phenotype, we examined the structure of amphid dendritic cilia by fluorescence and electron microscopy: point mutants displayed a significantly shorter cilium compared with wild-type worms, suggesting that the missense variant impacts on CHE-12-mediated ability to regulate ciliary MTs. Again, cilium shortening was less pronounced compared with the C-end deletion strain, further supporting its hypomorphic effect. Interestingly, nematodes that are hemizygous for the Arg284Trp variant displayed a further shortening of ASER dendritic cilium compared with wild-type animals. All these findings were corroborated by EM data that showed an evident ultrastructural disorganisation of cilium, particularly in its distal portion.

The p.Arg368Trp amino acid change affects the domain involved in tubulin binding. In line with in vivo findings, in vitro MT polymerisation experiments using the purified murine wild-type and mutated versions of the TOG2 domain[10] showed faster MT polymerisation with the mutant domain, suggesting an alteration in tubulin binding activity compared with the wild-type domain. Considering the MT-regulatory role of CHE-12, it will be interesting to evaluate the presence of MT defects in *che-12* point mutants.

Our findings indicate that the *che-12* missense variant is associated with a phenotype consisting of a shorter primary cilium with altered ultrastructure in the amphid neuron, which impair the ability to concentrate lipophilic dyes, but not the chemotaxis behaviour on a NaCl gradient. In vitro analysis confirmed an altered tubulin binding activity, consolidating previous findings. Altogether, these results point towards a hypomorphic effect of the novel variant.

Concerning *TOGARAM1* nonsense variant, a significant transcript degradation by NMRD was excluded by cDNA analysis from father's blood RNA (who is heterozygous for this allele) that showed a biallelic expression. This observation is line with the fact that NMRD efficiency is highly variable across transcripts, cells, tissues and individuals.[21]

Previous data obtained from distinct *che-12* mutants harbouring different C-end deletions downstream to the TOG2 domain clearly show that they all display a phenotype characterised by altered chemotaxis, dye filling defects and altered cilia,[9] and further works found that the whole *che-12* deletion mostly phenocopies these strains, although in a more penetrant way.[10]

The Arg1207 residue lies just before the TOG3 domain and, based on alignment data (online supplementary figure S2), is very close to the truncation of the nematode protein expressed by the *che-12(mn389)* mutant that hence was employed in our experiment.

It is possible to speculate that the region that is truncated in the Arg1207* mutant protein is required for MT binding; in fact, Das and coauthors[10] found that mutations affecting the TOG3 and TOG4 domains in the context of the full-length TOGARAM1 ablated the ability of the protein to localise to MT.

Remarkably, the majority of the genes associated with Meckel-Gruber and Joubert syndromes so far have orthologues in the *C. elegans* genome; they are specifically expressed in ciliated sensory neurons, as *che-12*.[22] Our work emphasises the usefulness of *C. elegans* as a multicellular model to validate novel variants potentially associated with human ciliopathies.

While we cannot predict the post-natal phenotype associated with biallelic *TOGARAM1* mutations, the affected fetuses do show a wide spectrum of defects overlapping in part the Meckel-Gruber syndrome phenotypes, including cleft of the lip and palate, microphthalmia, cerebral dysgenesis and hydrocephalus, in the absence of other key features as encephalocele, kidneys' cystic dysplasia and postaxial polydactyly.

Our data strongly support the role of *TOGARAM1* as a novel causative gene of primary ciliopathy, which thus should be included in diagnostic gene panel for this heterogeneous group of disorders. Additional studies are warranted for a deeper characterisation of the clinical spectrum of this disorder.

Author affiliations
[1]Clinical Genetics Unit, Department of Women's and Children's Health, University of Padova, Padova, Italy
[2]Laboratorio di Genetica ed Epidemiologia Clinica, Instituto di Ricerca Pediatrica Citta della Speranza, Padova, Italy
[3]Laboratory of Medical Genetics, Ospedale Pediatrico Bambino Gesù, Roma, Italy
[4]Department of Biology, University of North Carolina at Chapel Hill, Chapel Hill, North Carolina, USA
[5]Department of Oncology and Molecular Medicine, Istituto Superiore di Sanità, Roma, Italy
[6]Genetics and Rare Diseases Research Division, Ospedale Pediatrico Bambino Gesù, Roma, Italy
[7]Medical Genetics Unit, Azienda Ospedaliera Universitaria Città della Salute e della Scienza di Torino, Torino, Italy
[8]Scientific Directorate, Ospedale Pediatrico Bambino Gesù, Roma, Lazio, Italy

Acknowledgements We appreciate the kind cooperation of the family. We thank the technical support from Drs F Caicci and F Boldrin of DeBio, the Imaging Facility at the University of Padova (https://www.biologia.unipd.it/servizi/servizi-alla-ricerca/servizi-dipartimentali/imaging-facility/).

Contributors VM conceived and carried out the main bulk of experiments with *C. elegans*, with help from LP, who also contributed with genome editing to generate the point mutant worm lines. EA performed and interpreted the genetic analyses. KS carried out the in vitro studies with the mutant protein and performed structural modelling. DZ, EG and GG reported the clinical history of the family. MC performed the statistical analyses. LS helped to interpret the results. BD and AN assisted EA with genetic studies and critically revised the manuscript. SM proposed the experiment in discussions with VM and ET, provided critical feedback, and helped to shape the research and to analyse the manuscript. ET conceived and planned the experiments, supervised the findings of this work and wrote the manuscript with input from all authors. All authors discussed the results and contributed to the final manuscript.

Funding This research was supported by grants from Istituto di Ricerca Pediatrica (IRP) (to ET and LS) and the Italian Ministry of Health (GR-2016-02362779) (to ET), Vite Coraggiose (to AN, EA and BD), the Italian Ministry of Health (Ricerca Corrente 2019 to AN, EA) and "UNC Mosley Fund" (to KS).

Competing interests None declared.

Patient consent for publication Not required.

Provenance and peer review Not commissioned; externally peer reviewed.

Data availability statement Data are available on request.

ORCID iD
Eva Trevisson http://orcid.org/0000-0002-5380-6265

REFERENCES

1 Reiter JF, Leroux MR. Genes and molecular pathways underpinning ciliopathies. *Nat Rev Mol Cell Biol* 2017;18:533–47.
2 Bettencourt-Dias M, Hildebrandt F, Pellman D, Woods G, Godinho SA. Centrosomes and cilia in human disease. *Trends Genet* 2011;27:307–15.
3 Mirvis M, Stearns T, James Nelson W, structure C. Cilium structure, assembly, and disassembly regulated by the cytoskeleton. *Biochem J* 2018;475:2329–53.
4 Hildebrandt F, Benzing T, Katsanis N. Ciliopathies. *N Engl J Med* 2011;364:1533–43.
5 Bachmann-Gagescu R, Dempsey JC, Bulgheroni S, Chen ML, D'Arrigo S, Glass IA, Heller T, Héon E, Hildebrandt F, Joshi N, Knutzen D, Kroes HY, Mack SH, Nuovo S, Parisi MA, Snow J, Summers AC, Symons JM, Zein WM, Boltshauser E, Sayer JA, Gunay-

J Med Genet: first published as 10.1136/jmedgenet-2020-106833 on 3 August 2020. Downloaded from http://jmg.bmj.com/ on June 12, 2025 at Ist. Superiore Sanita Biblioteca. Protected by copyright, including for uses related to text and data mining, AI training, and similar technologies.

Aygun M, Valente EM, Doherty D. Healthcare recommendations for Joubert syndrome. *Am J Med Genet A* 2020;182:229–49.
6 Wheway G, Lord J, Baralle D. Splicing in the pathogenesis, diagnosis and treatment of ciliopathies. *Biochim Biophys Acta Gene Regul Mech* 2019;1862.
7 Devlin LA, Sayer JA. Renal ciliopathies. *Curr Opin Genet Dev* 2019;56:49–60.
8 Thomas S, Boutaud L, Reilly ML, Benmerah A. Cilia in hereditary cerebral anomalies. *Biol Cell* 2019;111:217–31.
9 Bacaj T, Lu Y, Shaham S. The conserved proteins CHE-12 and DYF-11 are required for sensory cilium function in *Caenorhabditis elegans*. *Genetics* 2008;178:989–1002.
10 Das A, Dickinson DJ, Wood CC, Goldstein B, Slep KC. Crescerin uses a TOG domain array to regulate microtubules in the primary cilium. *Mol Biol Cell* 2015;26:4248–64.
11 Rehm HL, Bale SJ, Bayrak-Toydemir P, Berg JS, Brown KK, Deignan JL, Friez MJ, Funke BH, Hegde MR, Lyon E, Working Group of the American College of Medical Genetics and Genomics Laboratory Quality Assurance Commitee. ACMG clinical laboratory standards for next-generation sequencing. *Genet Med* 2013;15:733–47.
12 Brenner S. The genetics of Caenorhabditis elegans. *Genetics* 1974;77:71–94.
13 Stiernagle T. Maintenance of C. elegans. *WormBook* 2006:1–11.
14 Paix A, Folkmann A, Seydoux G. Precision genome editing using CRISPR-Cas9 and linear repair templates in C. elegans. *Methods* 2017;121-122:86–93.
15 Paix A, Folkmann A, Rasoloson D, Seydoux G. High efficiency, homology-directed genome editing in *Caenorhabditis elegans* using CRISPR-Cas9 ribonucleoprotein complexes. *Genetics* 2015;201:47–54.
16 Yu S, Avery L, Baude E, Garbers DL. Guanylyl cyclase expression in specific sensory neurons: a new family of chemosensory receptors. *Proc Natl Acad Sci U S A* 1997;94:3384–7.
17 Richards S, Aziz N, Bale S, Bick D, Das S, Gastier-Foster J, Grody WW, Hegde M, Lyon E, Spector E, Voelkerding K, Rehm HL, Committee A, ACMG Laboratory Quality Assurance Committee. Standards and guidelines for the interpretation of sequence variants: a joint consensus recommendation of the American College of Medical Genetics and Genomics and the Association for Molecular Pathology. *Genet Med* 2015;17:405–23.
18 Slep KC, Vale RD. Structural basis of microtubule plus end tracking by XMAP215, CLIP-170, and EB1. *Mol Cell* 2007;27:976–91.
19 Ayaz P, Ye X, Huddleston P, Brautigam CA, Rice LM. A TOG:αβ-tubulin complex structure reveals conformation-based mechanisms for a microtubule polymerase. *Science* 2012;337:857–60.
20 Inglis PN, Ou G, Leroux MR, Scholey JM. The sensory cilia of Caenorhabditis elegans. *WormBook* 2007:1–22.
21 Dyle MC, Kolakada D, Cortazar MA, Jagannathan S. How to get away with nonsense: mechanisms and consequences of escape from nonsense-mediated RNA decay. *Wiley Interdiscip Rev RNA* 2020;11:e1560.
22 Masyukova SV, Landis DE, Henke SJ, Williams CL, Pieczynski JN, Roszczynialski KN, Covington JE, Malarkey EB, Yoder BK. A screen for modifiers of cilia phenotypes reveals novel MKS alleles and uncovers a specific genetic interaction between osm-3 and NPHP-4. *PLoS Genet* 2016;12:e1005841.

J Med Genet: first published as 10.1136/jmedgenet-2020-106833 on 3 August 2020. Downloaded from http://jmg.bmj.com/ on June 12, 2025 at Ist. Superiore Sanita Biblioteca. Protected by copyright, including for uses related to text and data mining, AI training, and similar technologies.